Available online at www.sciencedirect.com
ScienceDirect
Nuclear Instruments and Methods in Physics Research A 579 (2007) 326–329
NUCLEAR INSTRUMENTS & METHODS IN PHYSICS RESEARCH Section A
www.elsevier.com/locate/nima

Optimizing the number of equivalent iterations of 3D OSEM in SPECT reconstruction of I-131 focal activities

Kenneth F. Koral[a,*], James N. Kritzmaan[a], Virginia E. Rogers[a], Robert J. Ackermann[a], Jeffrey A Fessler[b]

[a]*Department of Radiology, University of Michigan Medical Center, 3480 KresgeIII, Ann Arbor, MI 48109-0552, USA*
[b]*Department of Electrical Engineering and Computer Science, University of Michigan, 3411 EECS, Ann Arbor, MI 48109-2122, USA*

Abstract

To externally estimate the radiation dose to a tumor during therapy with I-131 radiopharmaceuticals, and its distribution, one must accurately estimate activity, and its distribution, by means of SPECT imaging. Our objective is to characterize the quantification of the total activity in focal targets and in their uniform background, and of the activity distribution within the targets, after 3D Ordered Subsets Expectation Maximization (OSEM) reconstruction with attenuation and scatter correction and no post smoothing, in the good-counting-statistics case. A cylindrical phantom containing seven spheres simulating tumors, ranging in volume from 209 to 4.2 cm^3, and filled with an I-131 water solution containing background, was imaged. A Siemens Symbia SPECT/CT scanner was used to acquire 128×128 projection images, employing 60 angles over 360°. With dynamic SPECT, 10 sequential acquisitions of 15 min duration each were obtained and each was reconstructed with particular values of the number of subsets and the number of iterations. Let the product of the number of subsets times the number of iterations equal the equivalent number of iterations, EI. The counts-to-activity conversion factor was derived from the average ratio of total count divided by true activity for the largest sphere at the largest value of EI. Then, for the activity of each sphere at each of the values of EI, we evaluated (1) the fractional variance (variance in estimate over true activity), (2) the fractional bias (average estimate bias over true activity) and (3) the fractional error (the root mean square error (RMSE) in the estimate divided by the true activity). The fractional bias and fractional variance were smaller for the larger spheres compared to the smaller (the fractional bias decreased faster with an increase in the fractional variance for them as well). The RMSE was dominated by the bias. The fractional error decreased as EI increased for all sphere sizes. The minimum average value was 25.8% and occurred for EI = 480 although that image had texture and was noisy. The average fractional error was already approaching that value by EI = 80 at 30.7%, and that image was less noisy. For the water background surrounding the spheres, the fractional error in the activity estimate varied but little with EI; its smallest value was 13.1% at EI = 480. The error in a measure of estimated sphere activity non-uniformity worsened as EI increased. (The OSEM initial guess of identical counts/voxel everywhere was perfect as far as uniformity for these uniform-activity targets.) Therefore, the EI to employ in reconstruction depends on the activity-estimation task of interest. Different dosimetric goals might best be met by employing different images generated at different values of EI.

PACS: 87.57.Gg

Keywords: Quantification; Activity quantification; SPECT; OSEM; I-131; I-131 total activity; I-131 activity uniformity

1. Introduction

To optimally use SPECT images in the process of accurately estimating the spatially averaged radiation dose absorbed by a tumor during therapy with an I-131 radiopharmaceutical, they must, primarily, accurately quantify the total activity within the tumor volume, because most of the energy deposition comes from local beta particles. They must also accurately quantify the activity *distribution* within the entire field of view, but that has a lesser impact on the estimate. In addition, the non-uniformity of the tumor dose distribution may be of interest clinically, and for SPECT images to optimally

*Corresponding author.
E-mail address: kenkoral@umich.edu (K.F. Koral).

0168-9002/$ - see front matter © 2007 Elsevier B.V. All rights reserved.
doi:10.1016/j.nima.2007.04.070

estimate that non-uniformity mainly requires an accurate estimate of the *activity distribution within the tumor*. The Ordered Subsets Expectation Maximization (OSEM) reconstruction algorithm [1] with a 3D model of the point-source response function (psrf) has been investigated for these purposes. Pan et al. [2] and Pretorius et al. [3] found resolution and quantification improvements with the algorithm for Tc-99 m. With I-131, 3D OSEM better recovered the activity in small targets, compared to an algorithm with a 1D model. This fact was shown employing six subsets and 100 iterations to reconstruct projections from a seven-sphere phantom acquired by a Marconi Prism camera [4]. However, for the smaller spheres, not enough counts were placed within the geometric volumes of interest (VoIs) by the OSEM algorithm to recover their true activity completely [4,5]. Also, the SPECT image became artifactually structured and noisy under those reconstruction conditions, and so a registered CT image was a prerequisite for interpretation and the quantification.

Questions left unanswered by that study were:

- What was the variance of each activity estimate?
- Was the number of subsets and iterations optimum for activity recovery?
- What was the appearance of the bias-variance curve for the different spheres as the number of equivalent iterations (EI) increased?

Above, EI equals the product of the number of subsets times the number of iterations. Results are approximately the same for a particular EI value independent of how it is reached. Herein, we address the above questions. We also examine the accuracy of a measure of the uniformity of the activity distribution within the spheres. Possible deterioration of the quality of the results with lower counting statistics is not addressed, since counting statistics are usually good for intra-therapy measurements.

2. Methods

A cylindrical phantom with an elliptical cross-section that contained seven spheres simulating tumors, ranging in volume from 209 to 4.2 cm^3, and filled with an I-131 water solution, was imaged. Activity concentration was approximately the same in each sphere and the activity in the largest was 244 μCi. The activity concentration in the water in the spheres was approximately in the proportion of 5 to 1 to the activity concentration in the water in the cylinder. This latter concentration simulated tissue background. A Siemens Symbia SPECT/CT multi-modality imager acquired 128×128 projection images, employing 60 angles over 360°. A standard high-energy parallel-hole collimator was employed. Using dynamic SPECT, we obtained 10 sequential acquisitions of 15 min duration each, as well as an initial CT image. Reconstruction was carried out with the Siemens' software. The OSEM algorithm used a constant-value initial guess. The psrf of I-131 consists of a complex hexagonal-hole-pattern distribution for the main part of the response plus a siX-ray septal-penetration star pattern. The Siemens' depth-dependent model consisted of a rotationally symmetric Gaussian and, therefore, fit the local average of the count distribution. Attenuation correction was based on energy extrapolation of the CT values in the automatically superimposed CT image. The scatter corrupting the photopeak-window counts was estimated using the triple-energy-window method and was incorporated into the reconstruction. No post-reconstruction smoothing was employed. VoI corresponding to the geometric size of the interior of each sphere were located on the CT image and then used on the superimposed SPECT image to define the sphere volume. Similarly, a VoI for the phantom itself was defined and used. A counts-to-activity conversion factor was derived from the average ratio of total count divided by true activity for the largest sphere. From the repeat measurements of the phantom, we calculated the variance and average bias of the activity estimate for each sphere, at each EI. We also computed the root mean square error (RMSE) as a function of EI. This statistic is defined as

$$\mathrm{RMSE} = \sqrt{\left(\frac{1}{10}\sum (A_i - A)^2\right)}$$

where A_i is the ith estimate of a variable, and A is its true value. It can be computed from the variance of the estimate, V, and the average bias in the estimate, $\bar{B}$, as follows:

$$\mathrm{RMSE} = \sqrt{V + (\bar{B})^2}.$$

The bias in the ith estimate is defined as

$$B_i = A_i - A.$$

We also determined the fractional RMSE for the activity (the activity RMSE divided by the true activity). We then averaged the fractional RMSE values over all seven spheres, and looked for a minimum in the average as a function of EI. In addition, we calculated the fractional RMSE for the total activity in the water background. Finally, we calculated the coefficient of variation (COV) for the activity distribution within each sphere to serve as a measure of its non-uniformity. This statistic equals the relative standard deviation. Assuming that the true COV was zero, we determined the RMSE for the COV for each sphere as a function of EI.

3. Results

For the smallest sphere, the total count as a function of EI was quite varied for different experimental realizations of the same data, as shown in Fig. 1. The dependence for the next larger sphere was only somewhat similar, with the total count continuing to increase as EI increased for most of the realizations, but with a smaller slope compared to the large slope for several of the realizations with the

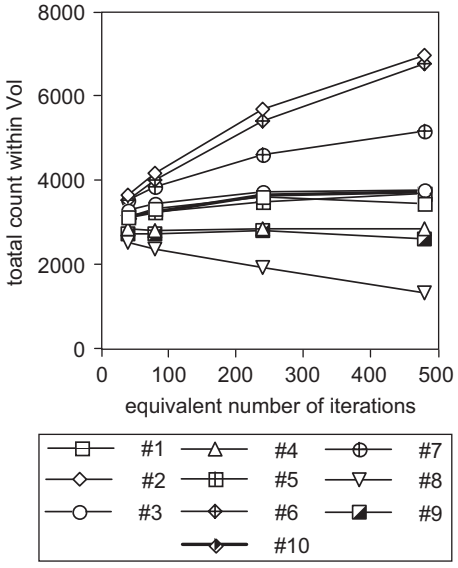

Fig. 1. Total-VoI-counts for 4.2 cm^3 sphere versus the equivalent number of iterations, EI. Dependence varied markedly with the realization number, given in the key to the plot.

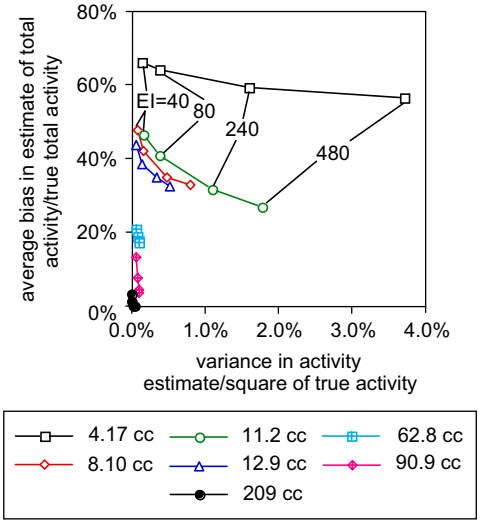

Fig. 2. Fractional bias versus fractional variance for each sphere size. The number of equivalent iterations, EI, for the data points for the 4.17 cm^3 and the 11.2 cm^3 sphere are shown. All sphere sizes follow that pattern.

smallest sphere. In addition, there was no instance of the count decreasing as EI increased. For larger spheres, there was much less variation between different realizations. The curve shape was that of a typical convergence, a fast increase followed by a slower approach toward an asymptote. Such convergence had been observed earlier for a 200 cm^3 sphere [6].

For the smallest sphere, the variance of the activity estimate worsened (increased) markedly as EI increased due to the results in Fig. 1, but the square of the average bias in the activity improved (decreased) fairly slowly. In absolute terms, the square of the average bias was much larger than the variance at all EI values. This caused the RMSE to improve, at least at a slow rate, as EI increased (this last result can be seen in Fig. 3). For the 90.9 cm^3 sphere, the variance of the activity estimate worsened quickly as the EI increased, but then did not worsen much more. The square of the average bias in the activity estimate improved rapidly as EI increased. The bias squared was much larger than the variance only for smaller EI values. Because of the leveling off of the variance at larger EI, the RMSE versus EI curve (again this can be seen in Fig. 3) looked somewhat similar to the curve for the square of the average bias versus EI, that is, it improved fairly rapidly.

In order to compare the bias-variance results from the seven spheres, we normalized the variance in the activity for each sphere by the square of its true activity, and normalized the average bias in the activity estimate for each sphere by its true activity. The results are presented in Fig. 2. Generally, at a given EI, the fractional bias and fractional variance were both smaller for the larger spheres than for the smaller spheres. Also, the fractional bias *decreased much faster* with an increase in the fractional variance for the larger spheres compared to the smaller ones.

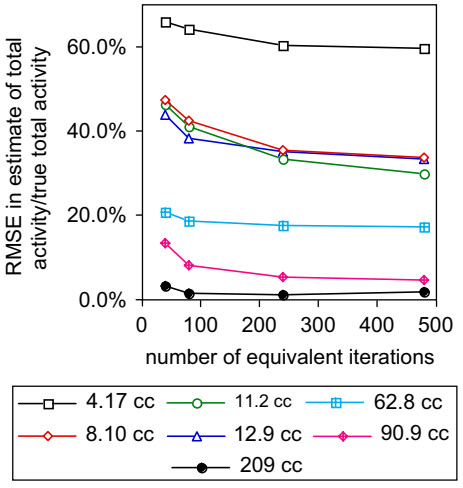

Fig. 3. The RMSE in the activity estimate as a percentage of the true activity as a function of the number of equivalent iterations, EI.

In order to compare the RMSE results from the different spheres, we plotted the fractional error in the estimate of total activity (the RMSE over the true activity) versus EI. This fractional error decreased as EI increased for all sphere sizes, as shown in Fig. 3. The smallest value for the fractional error averaged over all sphere sizes was 25.8% at EI = 480 {EI = 480 was the greatest number of subsets (16) and iterations (30) allowed by the commercial software}. The average fractional error was already approaching this value of 25.8% by EI = 80, having a value equal to 30.7%. This is shown in Fig. 4. The smaller spheres were the reason the average values were as high as they were.

For the water background, the fractional error in the estimate of total activity varied only a little with EI over the EI range tested. Its smallest value was 13.1% at EI = 480.

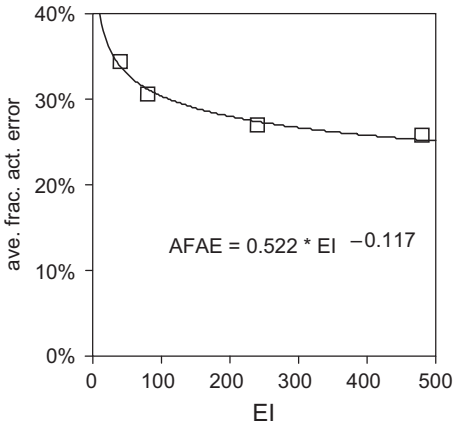

Fig. 4. Average fractional error, AFAE, versus EI.

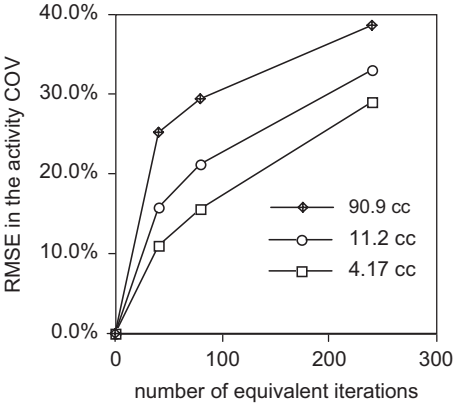

Fig. 5. Error in activity uniformity versus EI.

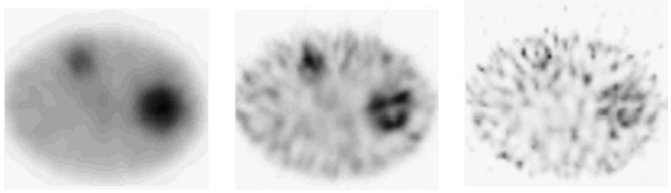

Fig. 6. Increase in noise and artifactual structure as EI increases. At left, with EI = 8 the image is smooth, the activity for the 209 cm^3 sphere (at 3 O'clock) is clearly stronger at the center, and that of the 62.8 cm^3 sphere (at 11 O'clock) is uniform. At middle, with EI = 80 the image is noisier and the larger sphere has artifactual structurre (a cold center). At right, with EI = 480 there is still more noise and the artifactual structure remains, or has arguably increased. (The 62.8 cm^3 sphere now appears to have a cold center.)

For all spheres, the accuracy of the activity COV worsened as EI increased. This occurred in part because the initial guess of identical counts/pixel everywhere is perfect as far as non-uniformity for targets that contain uniformly distributed activity as these did. There was a tendency, shown in Fig. 5, for the error to be larger as the sphere volume was larger. The images had increased small-scale structure, and also noise, as the EI value increased. This is shown by the results for a particular realization in Fig. 6. At higher EI, the VoIs for the larger spheres may have been big enough to encompass considerable structural variation whereas the VoIs for the smaller spheres perhaps did not to the same extent, leading to the larger error in the activity COV.

4. Conclusion

Using a multi-modality SPECT/CT scanner, the best number of EI for quantifying the total I-131 activity in spheres of various sizes is the maximum allowed by the software (EI = 480), even though the image then has considerable artifactual texture and is noisy. At EI = 80 (8 subsets, 10 iterations), the average fractional error in the estimate of total activity is almost as small (30.7% versus 25.8%), with a less-noisy image. The estimate of total background activity varies little from EI = 40 to 480. The results imply that EI = 480 is the optimum number of equivalent iterations of the commercial 3D OSEM algorithm to use for the purpose of estimating spatially averaged radiation absorbed dose to tumors using a SPECT/CT scanner. The accuracy of the spatial non-uniformity of the activity estimate for the measured spheres, which contained uniform activity, worsens as EI increases. This implies that the accuracy of the estimate of the non-uniformity of the dose distribution in a tumor probably would decrease as EI increased. Therefore, the EI to employ in reconstruction appears to depend on the dosimetric goal. This goal dictates the relative importance of various activity-estimation tasks. Using different images, from different values of EI, for different goals is a possibility.

References

[1] H.M. Hudson, L.S. Larkin, IEEE Trans. Med. Imaging 13 (4) (1994) 601.
[2] T.-S. Pan, D.-S. Luo, V. Kohli, M.A. King, Phys. Med. Biol. 42 (1997) 2517.
[3] P.H. Pretorius, M.A. King, T.-S. Pan, D.J. de Vries, S.J. Glick, C.L. Byrne, Phys. Med. Biol. 43 (1998) 407.
[4] K.F. Koral, A. Soni, A. Yendiki, Y. Dewaraja, Recovery of total I-131 activity within focal volumes using SPECT and 3D OSEM reconstruction, Phys. Med. Biol. 52 (2007) 777.
[5] K.F. Koral, A. Soni, A. Yendiki, Y.K. Dewaraja, J. Nucl. Med. 46 (Suppl. 2) (2005) Abstract book: pp. 106P-107P.
[6] K.F. Koral, A. Yendiki, Q. Lin, Y.K. Dewaraja, IEEE Trans. Nucl. Sci. 52 (1) (2005) 154–158.